MEMS capacitive force sensors for cellular and flight biomechanics

2007 Biomed. Mater. 2 S16

(http://iopscience.iop.org/1748-605X/2/1/S03)

INSTITUTE OF PHYSICS PUBLISHING BIOMEDICAL MATERIALS

Biomed. Mater. **2** (2007) S16–S22 doi:10.1088/1748-6041/2/1/S03

REVIEW ARTICLE

MEMS capacitive force sensors for cellular and flight biomechanics

Yu Sun[1] **and Bradley J Nelson**[2]

[1] Advanced Micro and Nanosystems Laboratory, University of Toronto, 5 King's College Road, Toronto M5S 3G8, Canada
[2] Institute of Robotics and Intelligent Systems, Swiss Federal Institute of Technology (ETH-Zürich), Zürich, Switzerland

E-mail: sun@mie.utoronto.ca

Received 27 November 2006
Accepted for publication 1 December 2006
Published 2 March 2007
Online at stacks.iop.org/BMM/2/S16

Abstract
Microelectromechanical systems (MEMS) are playing increasingly important roles in facilitating biological studies. They are capable of providing not only qualitative but also quantitative information on the cellular, sub-cellular and organism levels, which is instrumental to understanding the fundamental elements of biological systems. MEMS force sensors with their high bandwidth and high sensitivity combined with their small size, in particular, have found a role in this domain, because of the importance of quantifying forces and their effect on the function and morphology of many biological structures. This paper describes our research in the development of MEMS capacitive force sensors that have already demonstrated their effectiveness in the areas of cell mechanics and *Drosophila* flight dynamics studies.

1. Introduction

Measurements of minute forces at the μN (10^{-6} newton), nN (10^{-9} newton), and pN (10^{-12} newton) levels are crucial for understanding the fundamental elements of biological systems. Fundamentally, there are a few mechanisms used to measure an unknown force: (1) balancing the unknown force against a standard mass through a system of levers, (2) measuring the acceleration of a known mass, (3) equalizing it to a magnetic force or an optical force generated by the interaction of a current-carrying coil and a magnet or by the interaction of a laser beam and a trapped bead, (4) distributing the force on a specific area to generate pressure and then measuring the pressure, based on which force is indirectly derived, and (5) converting the applied force into the deformation of an elastic element. In the case of MEMS (microelectromechanical systems) capacitive force sensors, very small deflections caused by applied forces are transduced into detectable capacitance changes. An electronic circuit converts the capacitance variations into dc-voltage variations.

With their ability to measure forces from mN (10^{-3} newton) to pN, MEMS capacitive force sensors are suitable for a range of biological studies. Due to their high performance and their ability for multiple degree-of-freedom measurements, they are powerful alternatives to other MEMS transducers, such as cantilever-based sensors [1–3]. Compared to force measurement techniques, such as optical tweezers [4, 5], ultrafine glass needles (also known as the microneedle technique) [6, 7], atomic force microscopy (AFM) [8–11], magnetic bead measurement method [12–14] and micropipette aspiration [15, 16], MEMS capacitive force sensors provide the following advantages: (1) they are capable of measuring a wide range of forces from mN down to pN while the measurement range of other techniques is often limited, (2) they are capable of providing force information along multiple axes, (3) they provide the most direct means of

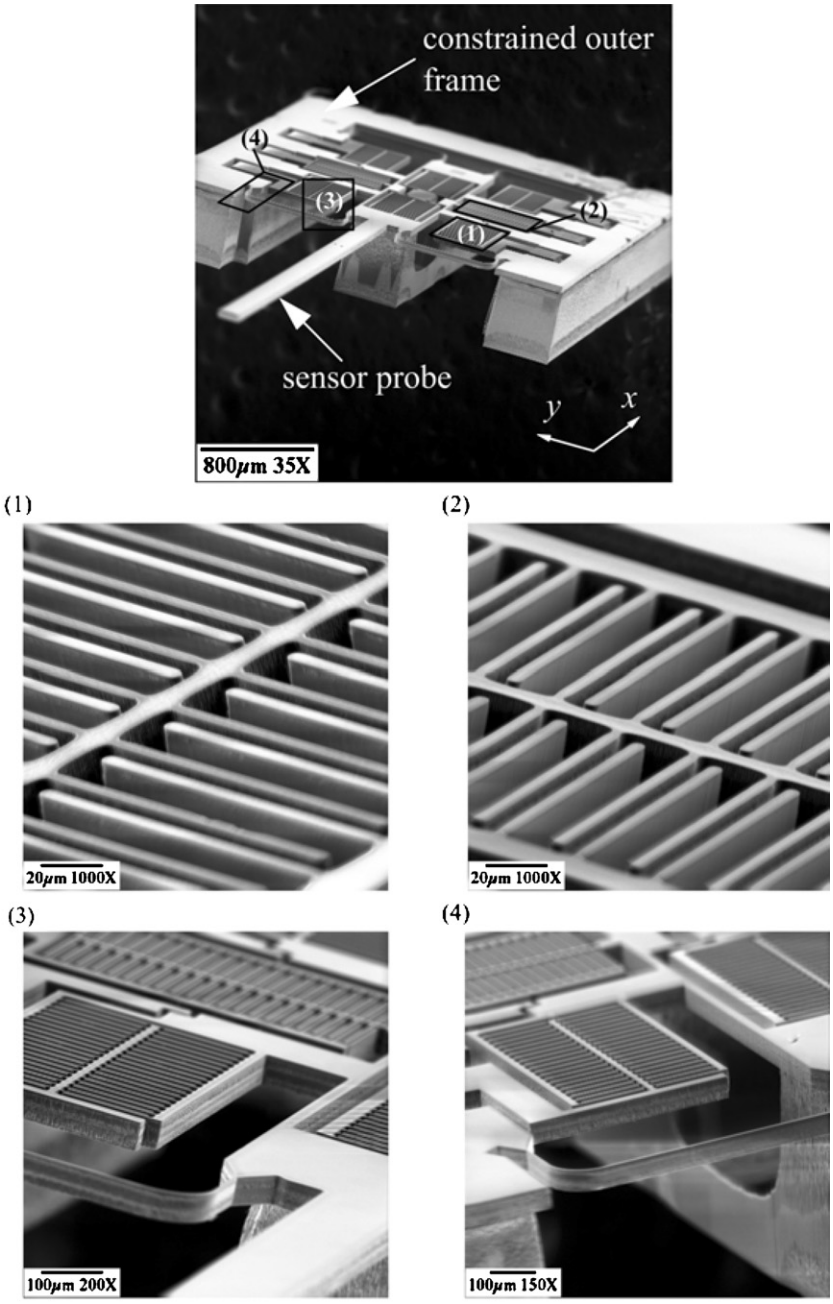

Figure 1. SEM picture of a two-axis MEMS cellular force sensor with four regions detailed.

force measurement instead of indirectly measuring pressure, (4) they have the advantage of low power, low noise, high sensitivity and insensitivity to temperature variation, and (5) batch microfabrication processes are capable of manufacturing hundreds of these transducers simultaneously, making them cost effective.

The rest of the paper presents two designs of MEMS capacitive force sensors and their applications for biological studies at the cellular and organism levels. It needs to be noted that the potential impact of MEMS capacitive force sensors extends beyond the presented applications by promising valuable tools for a broad range of biomechanical studies.

2. MEMS cellular force sensor and cell membrane mechanical property characterization

2.1. MEMS capacitive cellular force sensor

Two-axis capacitive cellular force sensors based on comb drives (i.e., a multitude of parallel-plate capacitors), as shown in figure 1, were constructed by a high-yield microfabrication process using DRIE (deep reactive ion etching) on SOI (silicon-on-insulator) wafers [17]. The device has a high sensitivity because of the large overlapping area. The sensitivity is further improved by adopting the transverse mode of comb drive movement that changes the gap between capacitor plates rather than the overlapping area.

The two-axis cellular force sensor is capable of resolving normal forces applied to a cell as well as tangential forces generated by improperly aligned cell probes. As shown in figure 1, the constrained outer frame and the inner movable structure are connected by four suspended silicon springs. A force applied to the probe causes the inner structure to move, changing the gap between each pair of interdigitated comb capacitors. Consequently, the total capacitance change resolves the applied force. The interdigitated capacitors are orthogonally configured to make the force sensor capable of resolving in-plane forces along both the x- and y-directions. The force-deflection model of the curved spring along both x and y is $\delta = \lambda \frac{F}{Ew^3t}$, where δ is the deflection, F is the applied force, $E = 100$ GPa is the Young's modulus of P-type $\langle 1\,0\,0 \rangle$ Si, w μm is the width of the springs, $t = 50$ μm is the height of the springs and $\lambda = 2.36 \times 10^{-10}$ m^3 along the x-direction and $\lambda = 1.1 \times 10^{-11}$ m^3 along the y-direction.

In order to fabricate the sensors, the microfabrication process starts with an SOI wafer (device Si layer 50 μm, SiO_2 layer 1 μm, handle Si layer 400 μm). *Step 1:* DRIE to form the features on the back side (the handle Si layer), *Step 2:* E-beam to evaporate Al to form ohmic contacts. Lift-off to pattern Al. Step *3:* DRIE the top side (device Si layer) to form capacitive comb fingers and springs. Step *4:* RIE (reactive ion etching) to remove the buried SiO_2 layer. The devices released onto a carrier dummy wafer below the device wafer, and were then picked up individually from the carrier dummy wafer. The dice-free release process protects fragile structures from damage. In the design and process, the handle layer Si is an integrated part of the force sensor, used for structural stability, dice-free releasing of the fragile structures, suspending the comb capacitors as well as mechanically connecting and electrically isolating capacitor plates.

A switched-capacitor-based capacitive readout circuit was used to convert a capacitance change into a voltage change. Calibration results demonstrate that the sensor is capable of resolving forces up to 25 μN in x and 110 μN in y with a resolution of 0.01 μN in x and 0.24 μN in y. Experimental results also demonstrated that these MEMS force sensors can be servoed to operate as an active force sensor. Due to the integrated electrostatic microactuators, device stiffness was modulated using force compensation, greatly increasing force measurement dynamic ranges. When the microforce sensor is actively servoed, an externally applied force is balanced by the electrostatic forces generated by the electrostatic microactuators within the sensor. The movable parts of the sensor are maintained in the equilibrium position, making the system a regulator system. The force measurement is obtained by interpreting the actuation voltages [18]. Additionally, it is also feasible to add in dedicated comb drives to actuate the sensor structure into resonance. The implementation of a capacitive *resonant* force sensor will further improve sensor resolution and stability, which is a topic of current research.

2.2. Cell membrane mechanical property characterization

Investigations into the functions and behaviour of various biological structures often require that the biomembranes isolating these structures from their immediate surroundings are characterized. The most common biomembranes are those composed of lipids and proteins, such as plasma membranes. Membrane lipids are organized in a bilayer that has two closely opposed sheets. Embedded in and associated with the lipid portion of the membrane are proteins. There are other types of biomembranes that have compositions different than lipid bilayer membranes. For example, the zona pellucida (ZP) is an extracellular biomembrane enveloping an oocyte. It is composed of three sulfated glycoproteins, called ZP-1, ZP-2 and ZP-3 that are synthesized by the oocyte.

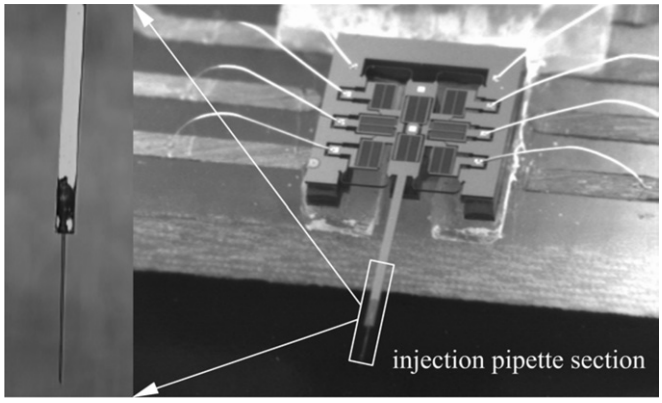

Figure 2. Wire-bonded cellular force sensor with an attached injection pipette section.

Upon fertilization, the ZP surrounding the oocyte undergoes a 'hardening' process in order to prevent subsequent sperm from penetrating. It has been speculated that ZP hardening is due to glycoprotein modification after fertilization. In cortical reactions occurring after fertilization, cortical granules undergo exocytosis as a result of an increase in the level of calcium, which modifies ZP glycoproteins resulting in ZP hardening. Some researchers deduce that the conversion of the zona pellucida glycoprotein ZP-2 to ZP-2f specifically contributes to ZP hardening [19]. ZP hardening has been assessed by comparing the duration of zona lysis in the presence of alpha-chymotrypsin [20]. However, there have been few studies investigating changes in the mechanical properties of the ZP post-fertilization.

To better understand the mechanical properties of mouse ZP and the mechanical property differences of ZP before and after fertilization, biomembrane force sensing has been conducted on mouse oocytes and embryos using the two-axis cellular force sensor.

2.2.1. Experiments. The cellular force sensor, wire bonded to a readout circuit board, was mounted on a motorized micromanipulator. Since tip geometry affects the quantitative force measurement results, a tip section of a standard ICSI (intracytoplasmic injection) injection pipette with a tip diameter of 5 μm was attached to the probe tip of the cellular force sensors, as shown in figure 2 in order to obtain valid biomembrane force information for ICSI studies.

Before the force sensor applies a uniaxial point load compressing the biomembrane and measures normal forces,

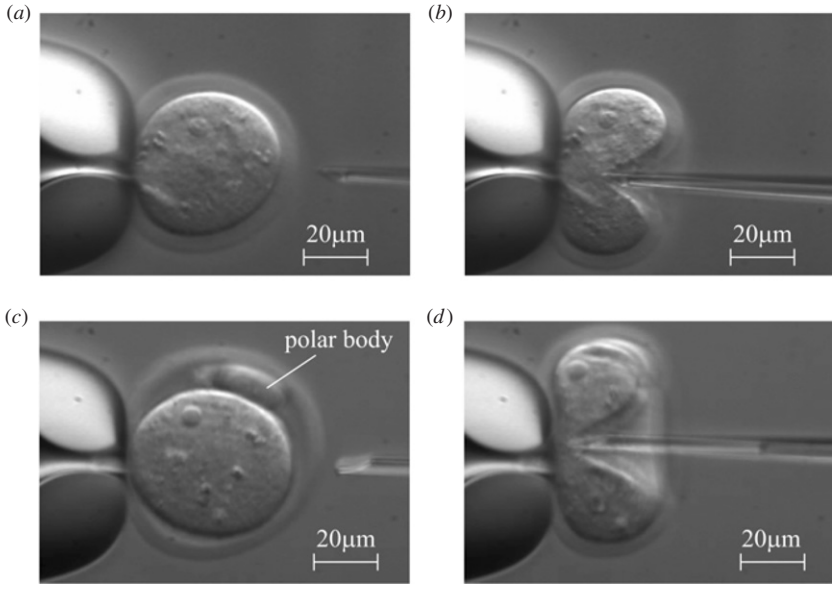

Figure 3. Force-displacement curve measurement. (*a*), (*b*) Mouse oocyte ZP. The applied force is 7.21 μN, and the indenter displacement is 42.2 μm. (*c*), (*d*) Mouse embryo ZP. The applied force is 12.7 μN and the indenter displacement is 52.3 μm.

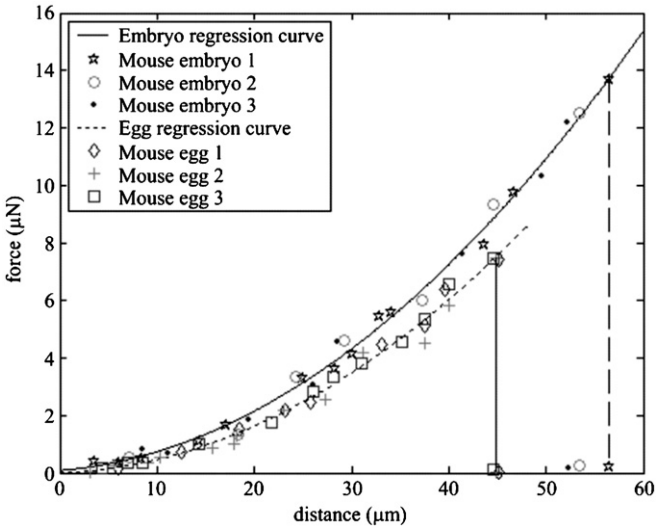

Figure 4. Force–deformation curves of mouse oocyte and embryo ZP.

the force sensor probe must be properly aligned such that tangential forces are minimized. This ensures that only a normal force is applied to the membrane. When the tangential force was minimized, normal forces and membrane geometry changes were captured.

2.2.2. Results and discussion. Figures 3(*a*) and (*b*) show the force and deformation measurement process on a mouse oocyte ZP. As shown in figure 4, forces increase nonlinearly as deformation increases. When deformation reaches about 45 μm, the ZP and the plasma membrane are punctured. The maximum membrane penetration forces are approximately 7.5 μN. After the force sensor tip punctures the membranes and travels into the cytoplasm, the force decreases rapidly, almost to zero. Figures 3(*c*) and (*d*) show the force and deformation measurement process on a mouse embryo ZP. The membranes are deformed as much as 53 μm before being punctured. The puncturing forces are approximately 13 μN, as shown in figure 4.

The experiments with the capacitive microforce sensor reveal that embryo membranes endure much larger deformations than oocyte membranes before being punctured. The required forces to puncture embryo membranes are almost twice as large as the forces for oocyte membranes. These measurement results quantitatively reveal the mechanical property differences that result from mouse ZP hardening. Detailed cell membrane mechanical modelling was described in [21].

This work has important implications for reproductive biologists working with *in vitro* fertilization and for biologists who develop transgenic organisms for biological research studies. The results provide additional evidence for protein cross-linking [22] that biologists have proposed as the mechanism by which zona hardening occurs.

3. MEMS capacitive microforce sensor and fruit fly flight force measurement

3.1. MEMS microforce sensor

The comb drive structure of the MEMS cellular force sensors presented in section 2.1 is equivalent to a two-plate capacitor model. Due to gap changes, the relationship between applied forces and resulting capacitance changes is nonlinear. This nonlinearity can be improved by adopting differential three-plate comb drives. In this case study, the MEMS microforce sensors using differential comb drives were developed for characterizing fruit fly (*Drosophila melanogaster*) flight behaviour.

Figure 5 shows the solid model of the microforce sensor design. The sensor probe transmits forces axially deflecting

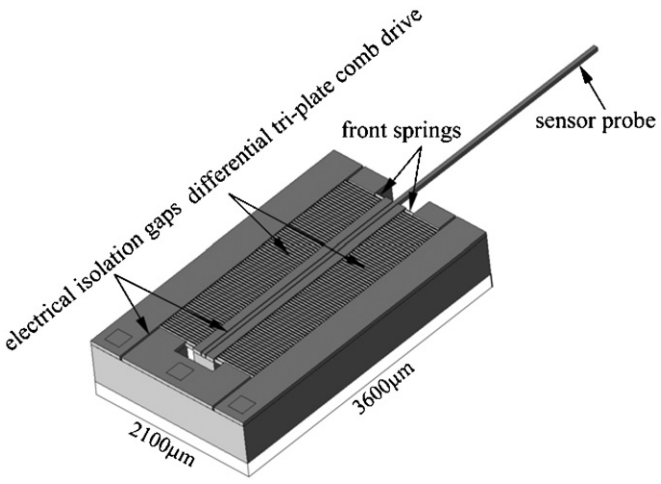

Figure 5. MEMS microforce sensor solid model.

the unidirectionally compliant springs. This deflection displaces the inner movable capacitor plates (2), shown in figure 6(*a*). With a force applied in the positive x-direction, plates (2) move away from plates (1) and closer to plates (3). When an ac signal is applied to the outer capacitors (plates (1) and (3)), a voltage divider is formed, as shown in figure 6(*b*). The resulting signal V_{out} is $V_{\text{out}} = V_s\left(\frac{C_1}{C_1+C_2}\right) - V_s\left(\frac{C_2}{C_1+C_2}\right)$ where $C_1 = K\varepsilon\frac{A_1}{d_1}$, $C_2 = K\varepsilon\frac{A_2}{d_2}$, plate area $A_1 = A_2$. The nominal plate spacing is $d_0 = \frac{d_1+d_2}{2}$. Defining $d_1 = d_0 + \Delta d$ and $d_2 = d_0 - \Delta d$, output can be shown as $V_{\text{out}} = V_s\frac{\Delta d}{d_0}$, which is linearly proportional to displacement.

By initially setting $d_1 = d_2 \ll d_3$, the undesired additional parallel capacitance effect can be minimized and linearity is maintained. System stiffness is determined by spring dimensions. By modelling the two straight springs in front shown in figure 6(*a*) as one spring constrained on both sides with a point load applied in the middle, the force–deflection model of a single spring is $\Delta d = \frac{Fl^3}{4Ew^3t}$ where F is the applied force, $E = 100$ GPa is Young's modulus of P-type $\langle 1\,0\,0\rangle$ silicon, and l, w and t are spring length, width and thickness respectively.

These sensors were microfabricated using the same DRIE on the SOI process described in section 2.1. The comb capacitor plates are also 50 μm in depth. An aspect ratio of 20 can be achieved using the microfabrication process, which requires only three lithographic masks. Figure 7 shows an SEM picture of a completed device. The sensors have a sensitivity of 1.35 μN mV^{-1}, a resolution of 0.68 μN and a bandwidth of 7.8 kHz [23].

3.2. *Fruit fly flight force measurement*

The fruit fly (*Drosophila melanogaster*) is a model organism studied by biologists for almost a century, and possesses a highly developed flight control system that provides the insect with the capability to perform robust stable flight, as well as exceedingly rapid and precise turning manoeuvres. The neurophysiology and biomechanics are inextricably linked and must be considered at the systems level. Multimodal sensory input converges on only eighteen control muscles that are responsible for the fine tuning of wing motion for manoeuvring. Beyond its impressive flight behaviour, *Drosophila melanogaster* is completely autonomous, extremely small, highly robust and self-replicating. To better understand the biomechanics underlying fly flight, precise measurements of the flight forces of these tiny (3 mm long) insects must be obtained.

The MEMS microforce sensors have been applied to characterizing the flight forces produced by tethered fruit flies. In the experiments, individual flies were attached to the MEMS sensor probe using a well-controlled process to minimize the interference with their flight behaviour. Figure 8 shows a fruit fly tethered to the force sensor probe and the force sensor wire bonded to a PCB (printed circuit board). Data were collected from six fruit flies at a sampling rate of 5 kHz. As shown in figure 9, the measured signal is periodic with a fundamental frequency just above 200 Hz corresponding to the typical wing beat frequency of fruit flies. Figure 9 shows the average lift forces from four flies over the duration of the time-normalized stroke cycle based on a total of 2875 wing strokes. Within

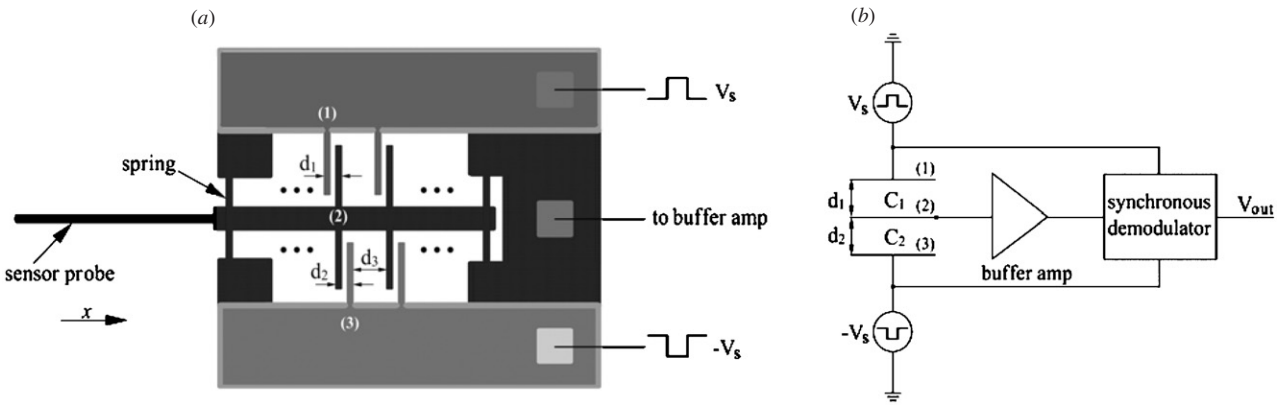

Figure 6. (*a*) Microforce sensor schematic. (*b*) Block diagram of sensor and readout circuit.

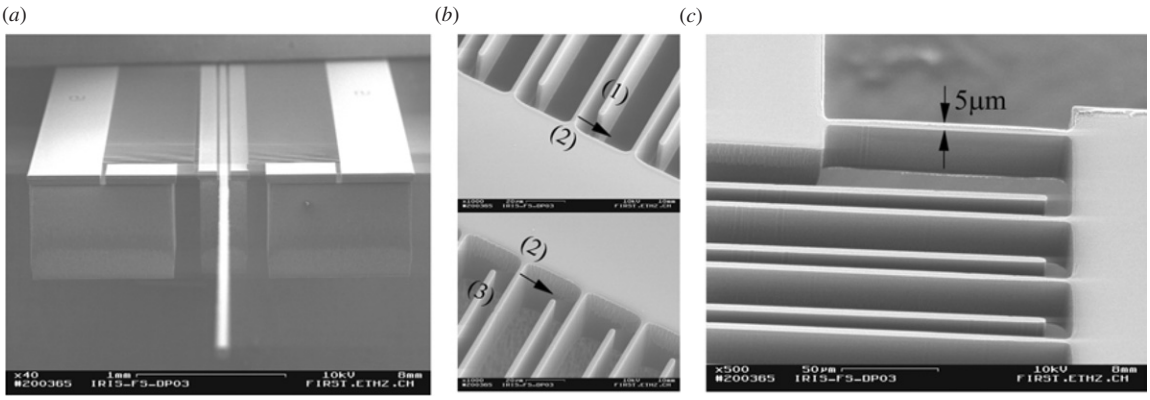

Figure 7. (*a*) SEM of a microforce sensor. (*b*) Differential three-plate comb drives. (*c*) Suspended spring and comb drives.

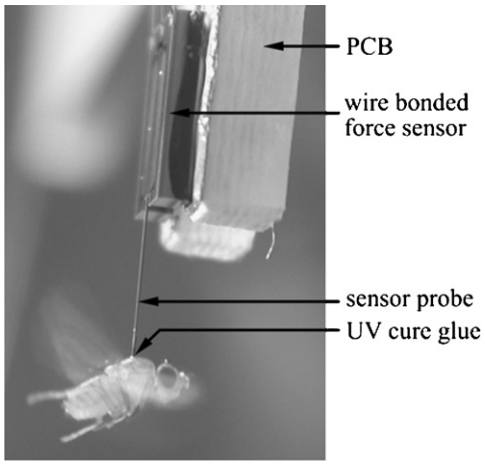

Figure 8. Flight force sensing of *Drosophila melanogaster* tethered to a MEMS microforce sensor probe.

each sequence, a contiguous section that showed little variance in wing beat frequency was chosen. The average lift force is 9.3 μN ($\pm$2.3 μN), which is in the range of typical body weights of fruit flies [23].

The MEMS microforce sensor provides a high sensitivity, broad range, small physical size, robustness and suitable geometry. The fruit fly flight force measurement results demonstrate the effectiveness of this technique for reliable and precise real-time measurements of flight forces in tethered flying fruit flies, promising important technological advance for flight biomechanical studies.

4. Conclusion

MEMS capacitive force sensors have found a role in quantifying force and its effect on the function and morphology of many biological structures. MEMS capacitive force sensors

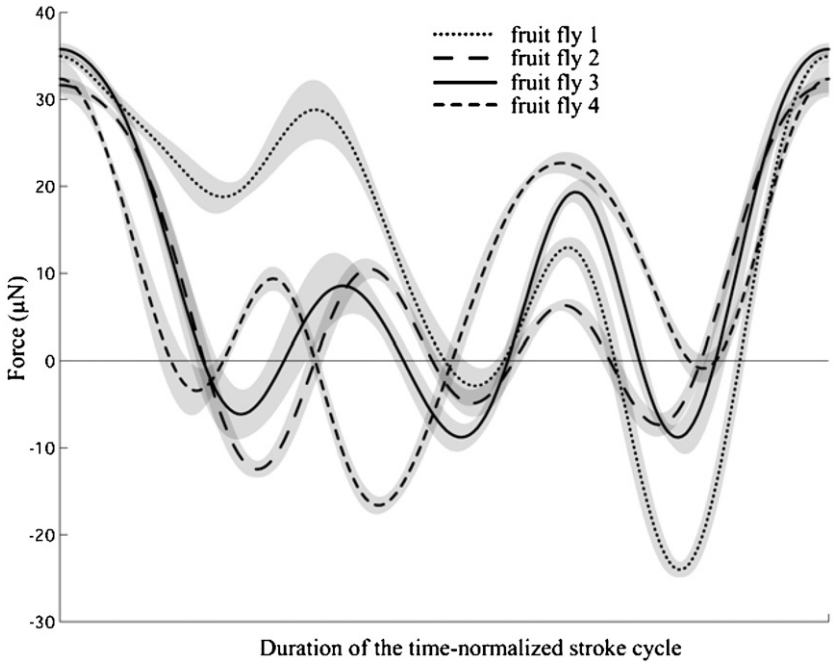

Figure 9. Flight lift forces over the duration of the time-normalized stroke cycle. The grey areas show 95% confidence intervals.

have already demonstrated their effectiveness in the areas of cell membrane biomechanics and *Drosophila* flight dynamics studies. Their high bandwidth, high sensitivity and large force measurement ranges combined with their small size make them well suited for many biological applications. Currently, these MEMS capacitive force sensors are limited to one or two degree-of-freedom measurements. The development of sensors for three or even six degrees of freedom with ultra-high resolutions of nN and pN is a topic of current research. Such devices will extend the range of applications and their value in biological research. Furthermore, as the ease of designing and fabricating these devices continues to improve, researchers will increasingly turn towards MEMS as standard tools for biology laboratories.

References

[1] Lin G, Pister K S and Roos K P 2000 Surface micromachined polysilicon heart cell force transducer *J. Microelectromech. Syst.* **9** 9–17

[2] Guilbault G G and Luong J H 1989 Biosensors: current status and future possibilities *Sel. Electrode Rev.* **11** 3–16

[3] Fauver M E, Dunaway D L, Lillenfeld D H, Craighead H G and Pollack G H 1998 Microfabricated cantilevers for measurement of subcellular and molecular forces *IEEE Trans. Biomed. Eng.* **45** 891–8

[4] Wright W H, Sonek G J, Tadir Y and Berns M W 1990 Laser trapping in cell biology *IEEE J. Quantum Electron.* **26** 2148–57

[5] Conia J, Edwards B S and Voelkel S 1997 The micro-robotic laboratory: optical trapping and scissing for the biologist *J. Clin. Lab. Anal.* **11** 28–38

[6] Kishino A and Yanagada T 1988 Force measurements by micromanipulation of a single actin filament by glass needles *Nature* **334** 74–6

[7] Ishijima A, Kojima H, Higuchi H, Harada Y, Funatsu T and Yanagida T 1996 Multiple and single-molecule analysis of the actomyosin motor by nanometer piconewton manipulation with a microneedle: unitary steps and forces *Biophys. J.* **70** 383–400

[8] Tokunaga M, Aoki T, Hiroshima M, Kitamura K and Yanagida T 1997 Subpiconewton intermolecular force microscopy *Biochem. Biophys. Res. Commun.* **231** 566–9

[9] Dammer U, Popescu O, Wagner P, Anselmetti D, Guntherodt H J and Misevic G N 1995 Binding strength between cell adhesion proteoglycans measured by atomic force microscopy *Science* **267** 1173–5

[10] Oberhauser A F, Marszalek P E, Erickson H P and Fernandez J M 1998 The molecular elasticity of the extracellular matrix protein tenascin *Nature* **393** 181–5

[11] Charras G T, Lehenkari P P and Horton M A 2001 Atomic force microscopy can be used to mechanically stimulate osteoblasts and evaluate cellular strain distribution *Ultramicroscopy* **86** 85–95

[12] Alenghat F J, Fabry B, Tsai K Y, Goldmann W H and Ingber D E 2000 Analysis of cell mechanics in single vinculin-deficient cells using a magnetic tweezer *Biochem. Res. Commun.* **277** 93–9

[13] Heinrich V and Waugh R E 1996 A piconewton force transducer and its application to measurement of the bending stiffness of phospholipids membranes *Ann. Biomed. Eng.* **24** 595–605

[14] Fass J N and Odde D J 2003 Tensile force dependent neurite elicitation via anti-β1 integrin antibody-coated magnetic beads *Biophys. J.* **85** 623–36

[15] Evans E 1999 Looking inside molecular bonds at biological interfaces with dynamic force spectroscopy *Biophys. Chem.* **82** 83–97

[16] Hochmuth R M 2000 Micropipette aspiration of living cells *J. Biomech.* **33** 15–22

[17] Sun Y, Nelson B J, Potasek D P and Enikov E 2002 A bulk microfabricated multi-axis capacitive cellular force sensor using transverse comb drives *J. Micromech. Microeng.* **12** 832–40

[18] Sun Y, Potasek D P, Piyabongkarn D, Rajamini R and Nelson B J 2003 *IEEE Int. Conf. Robot. Autom.* **1** 294–9

[19] Wassarman P M 1988 Zona pellucida glycoproteins *Ann. Rev. Biochem.* **57** 415–42

[20] Demeestere I, Barlow P and Leroy F 1997 Hardening of zona pellucida of mouse oocytes and embryos *in vivo* and *in vitro* *Int. J. Fertil. Womens Med.* **42** 219–22

[21] Sun Y, Wan K T, Nelson B J, Bischof J and Roberts K 2003 Mechanical property characterization of the mouse zona pellucida *IEEE Trans. Nanobiosci.* **2** 279–86

[22] Green D P L 1997 Three-dimensional structure of the zona pellucida *J. Reprod. Fertil.* **2** 147–56

[23] Sun Y, Fry S N, Potassek D P, Bell D J and Nelson B J 2005 Characterizing fruit fly flight behaviour using a microforce sensor with a new comb drive configuration *J. Microelectromech. Syst.* **14** 4–11